

Anomalous electrical transport behavior in the vicinity of the first-order magnetostructural transition in the giant magnetocaloric Gd_4ScGe_4

Y. Mudryk ^{1,*}, A. K. Pathak ², D. L. SchlageL ¹, T. A. Lograsso,¹ and V. K. Pecharsky ^{1,3}

¹The Ames Laboratory, U.S. Department of Energy, Iowa State University, Ames, Iowa 50011–2416, USA

²Department of Physics, SUNY Buffalo State, Buffalo, New York 14222, USA

³Department of Materials Science and Engineering, Iowa State University, Ames, Iowa 50011–1096, USA



(Received 20 January 2022; accepted 11 May 2022; published 31 May 2022)

Magnetic, specific heat, and electrical transport measurements of Gd_4ScGe_4 single crystals reveal sharp, discontinuous, nearly anhysteretic first-order magnetostructural transformation at $T_C = 63$ K. The electrical resistivity exhibits two distinct regions where it increases with decreasing temperature: between T_C and 120 K, as well as below 3 K; electronic transport remains conventionally metallic at all other measured temperatures, up to 325 K. The dispersion of charge carriers due to electron-paramagnon scattering is the likely reason for the observed anomalous transport above T_C . Additionally, the existence of intermediate lattice states near the transition recognized by the spike in the interslab Ge-Ge distances is expected to reduce the mean free path of the electrons contributing to the unusual behavior of the electrical resistivity between T_C and 120 K. Beyond conventional electronic and lattice terms, the third component of likely magnetic origin contributes to the low-temperature heat capacity; the presence of spin waves may be responsible for the increased electron-magnon scattering below 3 K. Minor magnetocrystalline anisotropy is observed with the b axis as the easy magnetization axis in Gd_4ScGe_4 . A negative deviation from linearity in the temperature dependence of the inverse magnetic susceptibility is detected below 150 K.

DOI: [10.1103/PhysRevB.105.174440](https://doi.org/10.1103/PhysRevB.105.174440)

I. INTRODUCTION

Examination of solids reacting reversibly and vigorously to external stimuli advances fundamental science by answering questions such as why a specific physical response occurs, what are the underlying mechanisms, and how the effect(s) can be enhanced, suppressed or replicated? Those solids are also important for applied science because they help to develop approaches to manipulate the responses and optimize relevant functionalities and identify ways to exploit them in a variety of energy systems and devices. Extraordinarily strong responsiveness of materials is commonly associated with discontinuous or nearly discontinuous phase transformations that can be triggered by rather weak external influences, such as minor variations of temperature, pressure or stress, and magnetic or electric fields.

Less common when compared with continuous, second-order phase transitions, first-order phase changes actuated by weak stimuli result in major and rapid variations of multiple physical parameters. For example, when the trigger is a variable external magnetic field, the most obvious, easily observable, and potentially functional result is sharp and substantial change of bulk magnetization. The latter is underpinned by major rearrangements that occur in a sublattice of individual magnetic moments, such as switching between magnetically disordered and ordered states, or reorienting the moment directions and changing magnetic structure. Further, when the magnetic lattice is strongly coupled to the

crystal structure, concerted magnetic and crystallographic transformations, as well as changes in the electronic structure and electrical transport behavior are often observed. There is ample evidence that robust magnetoelastic coupling realized in diverse material's systems, including ferromagnetic shape-memory alloys [1,2], perovskite-type manganites [3], and rare-earth intermetallic compounds [4–7], may lead to multifunctionality, such as giant magnetoresistive, giant magnetostrictive, and giant magnetocaloric effects, all observed in a single material [2–4].

The R_5T_4 family of compounds, where R is rare earth and T is group 13–15 elements (Ga, Si, Ge, Sn, Sb), is rich with representatives known to react actively to temperature, pressure, and magnetic field varying individually or together [7–9]. While not every R_5T_4 material is strongly responsive, those that are adopt peculiar crystallography, where a three-dimensional crystal lattice is built from distinctly two-dimensional atomic slabs stacked along the longest axis of its unit cell, usually the b axis (Fig. 1) [8]. Each of the slabs is a five-layer assembly, where the central flat atomic layer composed of R and T atoms is surrounded by two identical, densely populated, nearly flat layers of R atoms capped on both sides with loosely populated layers of T atoms. In this structure, the stacking of the slabs is flexible, controlled by variable interslab bonding that makes it possible for the lattice to adjust in response to external thermodynamic stimuli through shear displacements of the slabs with respect to one another. The shifts of neighboring slabs occur in opposite directions along the a axis, resulting in diffusionless, discontinuous first-order phase transformations [4]. Notably, the intraslab interatomic distances (and bonding) remain practically intact across such displacive transformations, but

*Corresponding author: slavkomk@ameslab.gov

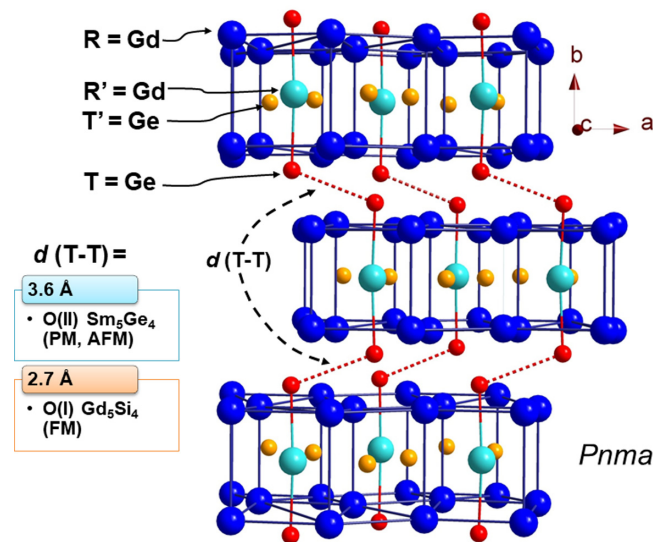


FIG. 1. Schematic illustrating unique crystallography of R_5T_4 compounds using Gd_5Ge_4 as an example. The main difference between the $\text{O(II)}\text{-Sm}_5\text{Ge}_4$ and $\text{O(I)}\text{-Gd}_5\text{Si}_4$ structure types constitutes breaking and forming of the interslab T - T bonds reflected by variable interatomic distances of, respectively, $d(T-T) = 3.6$ and $d(T-T) = 2.7 \text{ \AA}$.

the interslab distances and bonding change significantly. In particular, the interslab T - T bonds, highlighted in Fig. 1, can be either completely (every slab is displaced with respect to its neighbors) or half-broken/reformed (a slab is only displaced with respect to one of the neighboring slabs) across the transition (also see Fig. 9 for the temperature dependence of $d(T-T)$ in Gd_4ScGe_4), and this bond shuffling essentially determines both the atomic and magnetic structures within the R_5T_4 family [5,8].

The gadolinium germanide, Gd_5Ge_4 , is one of the most interesting among hundreds of known R_5T_4 compounds [5,10–14], even though one of its Si-substituted counterparts, $\text{Gd}_5\text{Si}_2\text{Ge}_2$, is the most studied to date due to the giant magnetocaloric effect it exhibits near room temperature [6]. Among many fundamentally interesting phenomena reported in Gd_5Ge_4 [15], low-temperature kinetic arrest and associated metastability are of particular importance. Nonequilibrium states that emerge at certain combinations of temperature and magnetic field affect the low-temperature physical behaviors of this compound, revealing strong history dependence and resulting in several unusual effects, such as magnetic deflagration [11,12].

Binary Gd_5Ge_4 adopts the Sm_5Ge_4 -type crystal structure at ambient conditions, also known as the O(II) type, where all of the interslab T - T bonds are long (broken), see Fig. 1. Upon cooling, paramagnetic (PM) Gd_5Ge_4 orders antiferromagnetically (AFM) at the Néel temperature, T_N , of 130 K, remaining AFM when cooled down to 1.8 K as long as the external magnetic field, H , remains below critical, H_{cr} , which varies between 10 and 15 kOe depending on the crystallographic orientation with respect to the magnetic field vector [8]. The increase of magnetic field above H_{cr} , however, triggers a discontinuous magnetostructural transformation from the AFM O(II) phase into the ferromagnetic (FM) phase with

a closely related Gd_5Si_4 -type crystal structure, also known as the O(I) -type, where all of the interslab T - T distances contract by nearly 1 \AA reflecting reformation of the corresponding bonds [5]. Remarkably, bonding between the nonmagnetic Ge atoms determines whether the material is FM or AFM, so in Gd_5Ge_4 the FM state is always associated with the O(I) structure, while both AFM and PM states are supported by the O(II) structure [5,10].

In addition to interesting magnetism, Gd_5Ge_4 shows an unusual yet so far not fully understood electronic transport. Levin *et al.* [13] reported that above T_N the temperature dependence of electrical resistivity, ρ , is nonmetallic, that is, ρ decreases with increasing temperature with the hopping conductivity as the likely mechanism, while in the magnetically ordered state the behavior is that of a metal. The negative $\partial\rho(T)/\partial T$ above T_N in Gd_5Ge_4 was independently confirmed by Szade and Skorek, who also revealed that between 300 and 400 K $\partial\rho(T)/\partial T \cong 0$ [16], as well as by Xue *et al.* [17], who found that the $\rho(T)$ behavior above T_N is not affected by the magnetic field, but it becomes anomalous at low-temperatures in $H = 20$ and 40 kOe, reflecting field-induced $\text{O(II)} \text{AFM} \leftrightarrow \text{O(I)} \text{FM}$ transitions. A number of first-principles calculations [13,18] point to a pseudogap at the Fermi level in the density of states (DOS) of Gd_5Ge_4 , which may be responsible for the nonmetallic behavior.

Partial substitution of Ge with Si removes the kinetic arrest present in the Gd_5Ge_4 parent, and the magnetostructural transition between the AFM-O(II) and FM-O(I) phases is no longer impeded in a zero magnetic field [19]. Sousa *et al.* presented a detailed investigation of the electrical resistivity behavior in the $\text{Gd}_5\text{Si}_{0.4}\text{Ge}_{3.6}$ compound [20], which is quite complex: on cooling from room temperature to T_N the resistivity increases, then starts decreasing similar to Gd_5Ge_4 , but there is a sharp increase in ρ when the temperature approaches T_C . A local maximum in $\rho(T)$ observed at T_C is followed by a rapid reduction of ρ down to 2 K. Repeated measurements indicate that cycling across T_C has little effect on the electrical resistivity below T_C , but it strongly affects the behavior above T_C – namely, a systematic rise in ρ is observed to the point where the peak at T_C disappears and the transition at T_C becomes manifested as a steep change in $\rho(T)$ for the 20th cycle and beyond.

Removal of the kinetic arrest can also be achieved by minor Sc for Gd substitutions [21,22]. Specifically, in the pseudobinary $\text{Gd}_{5-x}\text{Sc}_x\text{Ge}_4$ system stabilization of the ferromagnetic phase accompanied by the rise in T_C is observed when the concentration of scandium, $x(\text{Sc})$, remains below 1; when $x(\text{Sc}) > 1$ a dilution of the Gd sublattice by the nonmagnetic Sc weakens the magnetic exchange, gradually reducing both the molar magnetic moment and ferromagnetic ordering temperatures. The primary difference in the physical behavior between the Si-poor $\text{Gd}_5\text{Si}_x\text{Ge}_{4-x}$ and Sc-poor $\text{Gd}_{5-x}\text{Sc}_x\text{Ge}_4$ is vanishing of the global PM-AFM magnetic transition near $x(\text{Sc}) = 1$; the magnetostructural transition at T_C becomes order-disorder magnetically in Gd_4ScGe_4 , unlike order-order type in, for example, $\text{Gd}_5\text{Si}_{0.4}\text{Ge}_{3.6}$ [19,20]. The volume change at T_C is lower in Gd_4ScGe_4 , $\Delta V/V = 0.7\%$, when compared with the $\Delta V/V = 1.15\%$ in $\text{Gd}_5\text{Si}_{0.5}\text{Ge}_{3.5}$ [23]; however, the compound is still expected to be affected by significant strain/stress developing across the transformation boundary. The initial enhancement of ferromagnetism as the result of Gd/Sc substitution was, however, quite surprising,

and was explained by the enhanced hybridization of Sc $3d$ and Gd $5d$ states, a subsequent increase in the density of d states at the Fermi level (E_F) and, consequently, stronger mediation of $4f$ -electron exchange by the conduction electrons [21]. According to first-principles calculations [21], the enhancement of DOS near E_F also shifts the location of the pseudogap down to -1 eV below E_F for the majority and down to -0.6 eV for the minority spins, respectively, making it similar to Gd_5Si_4 [18] where electronic transport properties are metallic [16]. It is reasonable to assume that the lack of pseudogap near E_F will change the electronic transport of Sc-doped Gd_5Ge_4 .

The main goal of the current study is, therefore, to examine the effect of Sc substitution on the electronic transport of Gd_5Ge_4 . The Gd_4ScGe_4 composition was selected based on the results reported in Ref. [21]. Specifically: (1) among all $\text{Gd}_{5-x}\text{Sc}_x\text{Ge}_4$ compounds this optimally-doped Sc concentration has the highest $T_C = 65$ K; (2) the material is borderline first-order, exhibiting giant magnetocaloric effect with $\Delta S_{\text{max}} = -26$ J/kg K for $\Delta H = 20$ kOe at 67.5 K and negligible thermomagnetic hysteresis; (3) the first-principles calculations were performed specifically for this composition, allowing for direct comparison between theory and experiment; and (4) the temperature-dependent crystallography of Gd_4ScGe_4 has been established revealing a magnetostructural transition between the high-temperature O(II) and low-temperature O(I) polymorphs similar to $\text{Gd}_5\text{Si}_{0.4}\text{Ge}_{3.6}$ [19] and $\text{Gd}_5\text{Si}_{0.5}\text{Ge}_{3.5}$ [23] compounds. To minimize the influence of extrinsic effects often present in polycrystalline materials, we prepared a single-crystal Gd_4ScGe_4 compound using a triarc crystal pulling technique. Heat capacity and magnetic measurements were performed to complement and rationalize the electronic transport data.

II. EXPERIMENTAL

An approximately 4 cm long, 0.5 cm maximum diameter crystal of Gd_4ScGe_4 containing several large grains has been grown by the triarc crystal pulling method in a unit manufactured by Materials Research Furnaces Inc. using a 20 g charge prepared by arc-melting stoichiometric amounts of elemental Gd, Sc, and Ge. Gadolinium and scandium obtained from the Materials Preparation Center of Ames Laboratory were 99.8+ at. % pure with respect to all other elements in the periodic table. Germanium was purchased from Materion and was at least 99.999 wt.% pure with respect to the most common impurities (Cd, Cr, and Pb). The single crystal growth was initiated by dipping an $1/8''$ diameter tungsten seed rod into the center of the molten pool between the three arcs and then slowly lowering power until evidence of solidification around the edge of the seed was seen. The system was allowed to equilibrate at this state for approximately 10 min before withdrawing the seed at a rate of 0.254 mm/min. The growth interface was monitored, and the power was adjusted manually as needed to regulate the diameter of the pulled specimen. The obtained grains were crystallographically oriented by back-reflection Laue using a PANalytical PW1830 generator with a Photonic Science camera. Since it can be difficult to distinguish between the [100] and [001] crystallographic directions in the Gd_5Ge_4 systems by the Laue method alone, verification was done by x-ray diffraction using a PANalytical

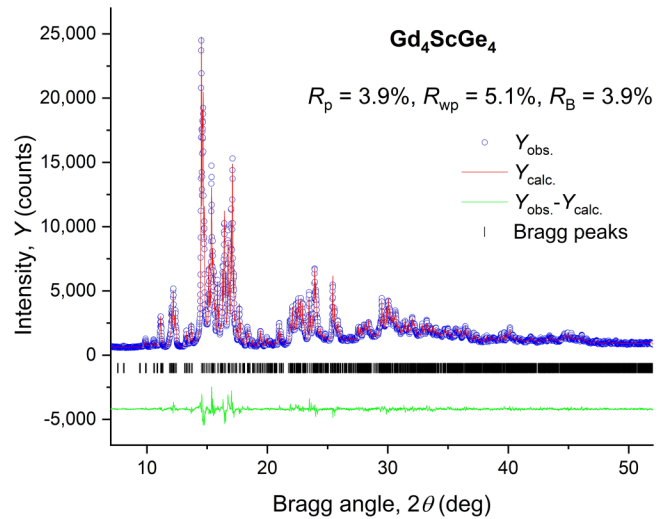


FIG. 2. Rietveld-refined x-ray diffraction pattern measured at room temperature using a powder prepared by grinding a piece of as-grown Gd_4ScGe_4 single crystal.

X'Pert Pro system, which confirmed that only the families of (h00), (0k0) or (00l) Bragg reflections were present in the diffraction patterns collected with standard θ - 2θ scans.

A specimen taken from the as-grown crystal was ground using a mortar and a pestle, and a powder diffraction pattern was recorded at room temperature using Mo $K\alpha$ radiation on the Rigaku TTRAX rotating anode diffractometer. The Rietveld refinement of the x-ray diffraction pattern was performed using FULLPROF [24], revealing phase-pure compound crystallizing in the O(II) (Sm_5Ge_4 -type) structure. The Rietveld-refined powder diffraction pattern is illustrated in Fig. 2 and derived crystallographic parameters are listed in Table I. The refinement of site occupancies indicates Gd-rich, off-stoichiometric composition $\text{Gd}_{4.19(1)}\text{Sc}_{0.81(1)}\text{Ge}_4$. One must, however, take into account that the least-squares standard deviations of free variables included in the Rietveld refinements are commonly underestimated because the number of experimental observations (intensity data points) is much higher than the number of Bragg peaks. Hence, the formal errors in the refined $\text{Gd}_{4.19(1)}\text{Sc}_{0.81(1)}\text{Ge}_4$ composition are likely 5 – 10 times higher. Further, the analysis of lattice parameters (Table I) also shows that the unit cell volume, V , of the Bridgman-grown crystal, $850.59(4) \text{ \AA}^3$, is slightly larger than $V = 846.11(8) \text{ \AA}^3$ of the polycrystalline sample reported in Ref. [21], confirming a minor increase of the Gd/Sc ratio in the former but pointing at a slightly different composition, $\text{Gd}_{4.1}\text{Sc}_{0.9}\text{Ge}_4$. Considering that physical behaviors of the single crystal studied in this work are quite similar to those of the polycrystalline Gd_4ScGe_4 examined in Ref. [21], we use the nominal Gd_4ScGe_4 stoichiometry throughout the manuscript.

Three parallelepiped-shaped crystals measuring $1.16 \times 1.71 \times 0.98 \text{ mm}^3$, $0.98 \times 1.71 \times 1.08 \text{ mm}^3$, and $1.71 \times 0.92 \times 0.98 \text{ mm}^3$ with the first dimension listed parallel, respectively, to [010], [001], and [100] crystallographic directions for magnetic property measurements were cut from the as-grown crystal using electrical discharge machining. Another parallelepiped measuring $7.55 \times 2.54 \times 1.31 \text{ mm}^3$ with the longest edge parallel to the [100] direction was cut

TABLE I. Crystallographic parameters obtained from the Rietveld refinement of the pattern illustrated in Fig. 2. The refined lattice parameters are $a = 7.5278(2)$ Å, $b = 14.6395(4)$ Å, $c = 7.7183(2)$ Å, and the calculated unit cell volume is $V = 850.579(4)$ Å³.

Atom	Wyckoff	x/a	y/b	z/c	Fractional occupancies, g^a
Gd1	4c	0.3055(7)	0.25	0.0047(6)	0.504(2)
Gd2	8d	0.0102(2)	0.5979(1)	0.1815(2)	1.0
Gd3	8d	0.1411(2)	0.1190(1)	0.3348(2)	0.841(3)
Sc1	4c	0.3055(7)	0.25	0.0047(6)	0.496(2)
Sc3	8d	0.1411(2)	0.1190(1)	0.3348(2)	0.159(3)
Ge1	4c	0.1882(6)	0.25	0.6357(7)	1.0
Ge2	4c	0.4450(7)	0.25	0.3870(6)	1.0
Ge3	8d	0.3034(6)	0.0448(2)	0.0317(5)	1.0

^aOverall occupancies of the Gd1/Sc1 and Gd3/Sc3 sites were constrained to maintain $g_{\text{Gd}} + g_{\text{Sc}} = 1.0$.

for the electrical transport measurements. The electrical resistivity was measured using a standard four-probe technique with the current applied along the [100] direction and the magnetic field applied along the [010] direction. Heat capacity data between 2 and 100 K were measured using the $1.71 \times 0.92 \times 0.98$ mm³ specimen, the same as used in the magnetic property measurements. An additional thin plate with the [010] axis normal to its surface was also extracted from the as-grown crystal and used in heat capacity measurements using the ³He system.

Magnetization measurements, both as a function of temperature, $M(T)$, and magnetic field, $M(H)$, were performed using a superconducting quantum interference device magnetometer (model MPMS XL-7, Quantum Design, Inc.) between 2 and 300 K and in applied magnetic fields up to 7 T. By using the formulas and tables of Chen *et al.* [25] the demagnetizing factors were calculated as 0.32, 0.40, and 0.22 for the crystals oriented along [010], [001], and [100], respectively. The demagnetization correction was applied to the $M(H)$ data using the $H_{\text{int}} = H_{\text{ext}} - N * M$, where H_{int} and H_{ext} are the internal and external magnetic fields, N is the demagnetizing factor, and M is the volumetric magnetization calculated using theoretical (x -ray) density determined from the crystallographic data of Table I. Heat capacity and electrical resistivity measurements were performed using a physical property measurement system (PPMS, Quantum Design, Inc.). The measurements were first performed using the standard attachments, then the ³He attachment was utilized to reach temperatures as low as 700 mK.

III. RESULTS

A. Magnetic measurements

As reported, polycrystalline Gd₄ScGe₄ orders magnetically, exhibiting a sharp, nearly discontinuous phase transition between the paramagnetic O(II)-type phase and the ferromagnetic O(I)-type phase at $T_C = 65$ K with negligible hysteresis [21]. Figure 3(a) shows minor differences between $M(T)$ of polycrystalline (from Ref. [21]) and two single-crystalline samples, the latter with the magnetic field applied parallel to [010] and [001] directions, all measured in $H = 1$ kOe. $M(T)$ data measured with the field applied along the [100] direction are similar to those of [010] and they are illustrated separately in Fig. 4(a).

The transition temperature of the single crystals, $T_C = 63$ K on heating for all directions measured, is 2 K lower compared to the polycrystalline sample of Ref. [21], reflecting higher Gd/Sc ratio, in accordance with the magnetic phase diagram of Ref. [21] and in agreement with x -ray powder diffraction data discussed above. Predictably, the single crystalline sample shows a sharper transition, but also displays a more distinct thermal hysteresis, ΔT_h , of about 2 K between the cooling and the heating branches. The presence of minor hysteresis further corroborates the slightly shifted toward the Gd-rich end composition of the single crystal because the borderline first-order type magnetic ordering transformation detected when $x = 1$ becomes more distinctly first-order when $x < 1$. At the same time, the observed $\Delta T_h = 2$ K remains much lower when compared to polycrystalline Gd_{5-x}Sc_xGe₄ compounds with $0.125 \leq x \leq 0.5$, for example $\Delta T_h = 10$ K when $x = 0.25$ [22].

Magnetocrystalline anisotropy was examined by measuring isothermal $M(H)$ data at $T = 2$ K after cooling the samples in a zero magnetic field. As seen in Fig. 3(b), differences between the three directions are minor, and [010] is the easy magnetization direction, same as that of the binary ferromagnetic Gd₅Ge₄ parent [26]. Since Gd³⁺ has no orbital magnetic moment, the weak magnetic anisotropy is present because both the room temperature O(II) and low-temperature O(I) orthorhombic unit cells are pseudotetragonal, with the b axis being approximately twice as long as the other two axes. Microscopically, the anisotropy was confirmed by X-ray resonant magnetic scattering experiments of the Gd₅Ge₄ parent, which showed that there is indeed a preferred orientation of magnetic moments along the slabs (the moments are confined within the ac plane) in the AFM state [27]. The saturated magnetization reaches 177 emu/g or 30.5 μ_B /f.u. at 70 kOe, which, assuming nonmagnetic Sc, leads to 7.64 μ_B /Gd. According to density functional theory calculations, the induced magnetic moment on Sc is 0.24 μ_B /atom [21]. Taking this into account, the experimentally determined moment per Gd atom becomes 7.58 μ_B . Compared to Gd₅Si_{0.5}Ge_{3.5} [23], which has a saturation moment of 7.50 μ_B /Gd, a minor enhancement of the moment is due to increased contribution from the spin-polarized Gd 5d electrons associated with the introduction of Sc into the lattice.

Isofield $M(T)$ data measured with the magnetic fields of 1 and 20 kOe applied along [100] direction are shown in Fig. 4(a), and the temperature dependencies of the inverse magnetic susceptibility (H/M) for the same applied fields –

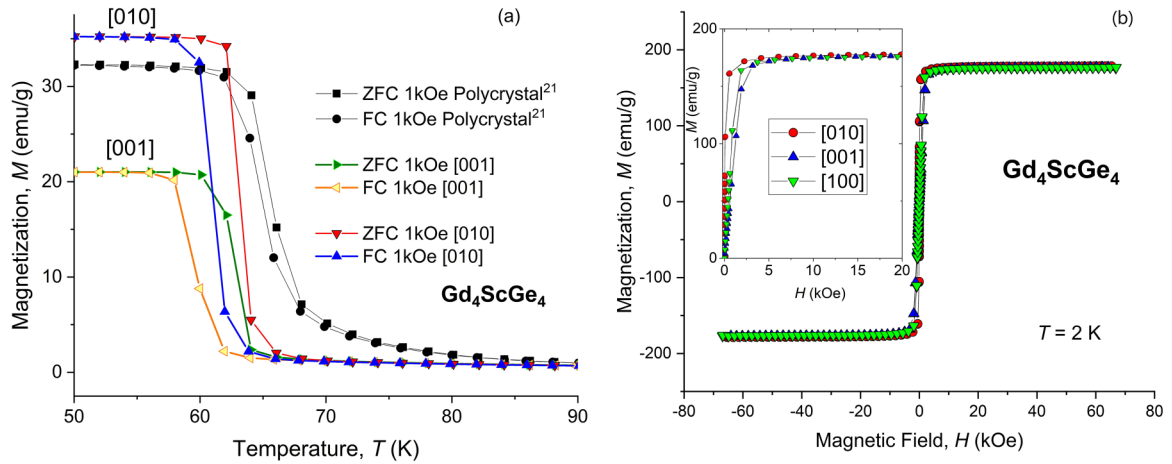


FIG. 3. (a) Zero-field cooling (ZFC) and field-cooled (FC) isofield magnetization, $M(T)$, in the vicinity of the magnetostructural transition for the [010] and [001] orientations of the Gd_4ScGe_4 crystal compared with the polycrystalline Gd_4ScGe_4 [21]. (b) Isothermal, $M(H)$, data at $T = 2$ K for the three crystallographic axes with the inset presenting an expanded view of the first quadrant.

in Fig. 4(b). The first-order character of the transition is preserved at 20 kOe, and the transition temperature is shifted up by 7 K, indicating $dT_C/dH = 0.35$ K/kOe, which is in line with $dT_C/dH \sim 0.4$ K/kOe rate typically observed in related Gd_5T_4 compounds with first-order magnetostructural transformations between the AFM or PM O(II) and FM O(I) structures [15]. The inverse susceptibility in the paramagnetic state follows the Curie-Weiss behavior in the whole measured range for the 20 kOe data, but one can note a negative deviation from the linearity in the 1 kOe data around 150 K, which is commonly associated with short-range correlations, known as the Griffiths-like phase region [28–30]. The negative deviation becomes more pronounced in lower applied magnetic fields, for example, 50 Oe, as illustrated in the inset of Fig. 4(b) and in the ac susceptibility measurements (not shown). The Curie-Weiss fit reveals the Weiss temperature, $\theta_p = 33$ K, and the effective magnetic moment, $p_{\text{eff}} = 8.2 \mu_B/\text{Gd}$, which is higher than the $7.94 \mu_B/\text{Gd}$ expected for noninteracting Gd^{3+} . We note that here we assume zero Sc

moment in the PM state, the induced, due to spin-polarization, Sc moment mentioned above is for the FM-ordered state. The slightly enhanced value of p_{eff} shows that there is a minor contribution to the total moment in the paramagnetic state that comes from the conduction electrons, but scandium is likely nonmagnetic.

Temperature-dependent ac magnetic susceptibility measurements (not shown) agree with the $M(T)$ data confirming the sharp PM-FM transition at T_C . A minor, weakly frequency-dependent anomaly, is observed at 20 K and is likely related to the remnant metastability associated with the kinetic arrest known to occur in the parent Gd_5Ge_4 [11], but it does not correlate with any other physical behaviors measured and reported here.

B. Heat capacity

First, the heat capacity of Gd_4ScGe_4 was measured between 2 and ~ 95 K and the data show a sharp peak at $T_C =$

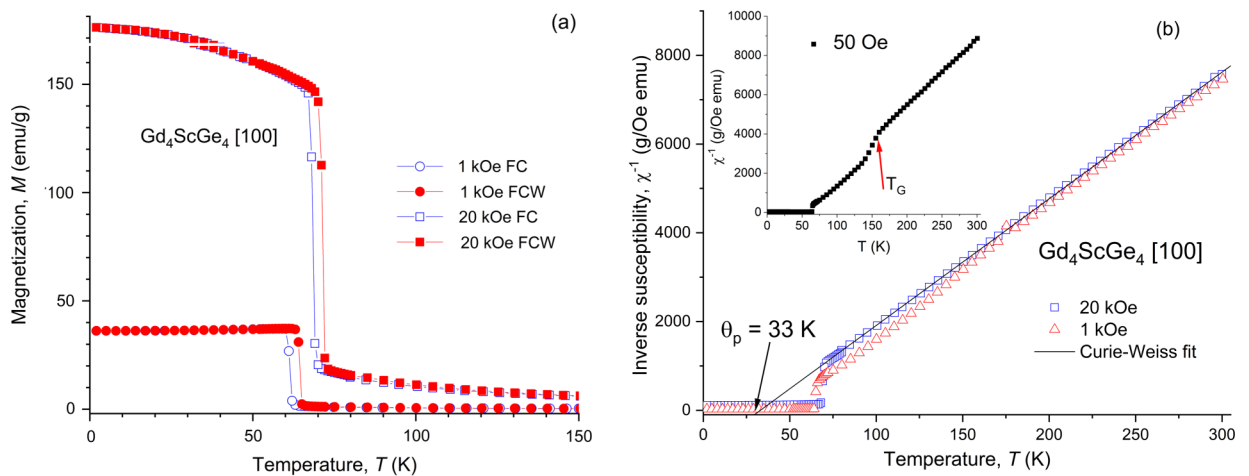


FIG. 4. (a) Field-cooled (FC) and field-cooled warming (FCW) isofield magnetization, $M(T)$, of Gd_4ScGe_4 measured at the magnetic fields 1 and 20 kOe applied along the [100] direction. (b) Inverse magnetic susceptibility ($\chi^{-1} = H/M$) calculated from the data presented in (a), showing the Curie-Weiss fit of the 20 kOe data. Inset in (b) shows inverse magnetic susceptibility measured in a 50 Oe magnetic field, highlighting notable deviation from linearity near $T_G \sim 150$ K.

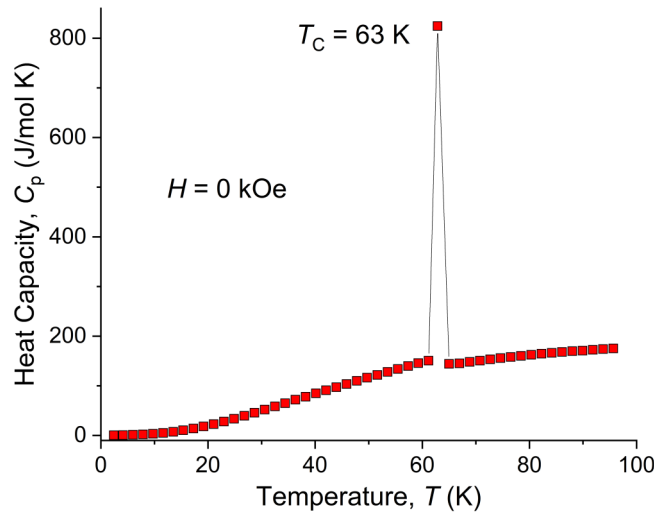
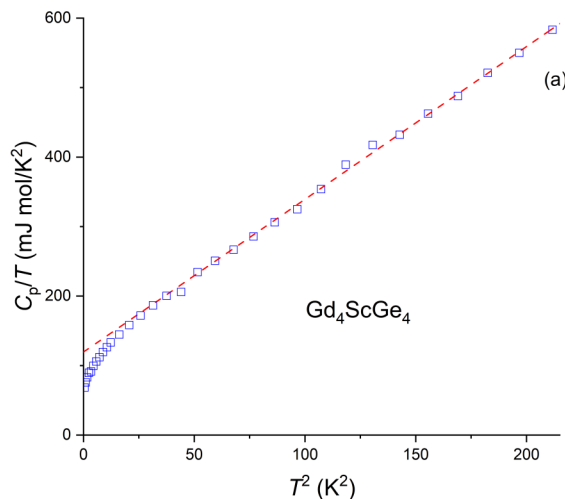


FIG. 5. Heat capacity of Gd_4ScGe_4 measured in zero applied magnetic field between 2 and ~ 95 K. The line is a guide for the eye.

63 K (on heating), which unambiguously defines the transition as first order (Fig. 5). No other anomalies are observed in the studied temperature range.

Next, we collected heat capacity data in the temperature range between 0.7 and 15 K. The $C_p(T)$ plot illustrated in Fig. 6(b) exhibits no obvious anomalies in this temperature range. Given that the studied material shows metallic properties below T_C , see next section, we attempted to fit the data using the $C_p(T) = \gamma T + \beta T^3 + \delta T^n$ equation [31], where γT represents the electronic heat capacity, βT^3 are lattice vibrations in the Debye approximation, and δT^n are spin-wave excitations or magnetic contributions. The fit with all parameters unrestrained yields physically unrealistic values with very large uncertainties (not shown; here and below the uncertainties are taken as the least-squares standard deviations).

The C_p/T vs T^2 plot illustrated in Fig. 6(a) clearly shows nonlinear behavior below $T^2 = 50 \text{ K}^2$ (corresponding to $T <$



~ 7 K). Similar behaviors were observed in metallic Gd [32] and intermetallic Gd_5Ge_4 [13] and were attributed to the presence of the magnetic δT^n term. The downward curvature is more pronounced in the title material when compared to Gd_5Ge_4 [13], although it may simply be due to the fact that our data extend down to 0.7 K. Because the C_p/T vs T^2 plot is obviously nonlinear below 7 K, one can safely assume that there is, indeed, another contribution to the total specific heat in addition to the electronic and lattice terms.

With this in mind, we fitted the heat capacity data with $C_p(T) = \gamma T + \beta T^3 + \delta T^n$ equation assuming $n = 3/2$, which is expected for the metallic ferromagnetic materials (see, for example, analysis of the heat capacity of elemental Gd by Hill *et al.*) [32]. Keeping n as a constant, we obtained much lower fit uncertainties and the fit results in the following parameters: $\gamma = 50 \pm 11 \text{ mJ}/(\text{mol K}^2)$, $\beta = 1.97 \pm 0.04 \text{ mJ}/(\text{mol K}^4)$, and $\delta = 30 \pm 5 \text{ mJ}/(\text{mol K}^{5/2})$. The Debye temperature, θ_D , calculated from β , is 207 ± 5 K. By dividing the values of γ and δ parameters per number of atoms in the formula unit, we obtain $\gamma = 5.5 \pm 1.3 \text{ mJ}/(\text{g-at K}^2)$ and $\delta = 3.32 \pm 0.58 \text{ mJ}/(\text{g-at K}^{5/2})$ and now can compare these values with those obtained for the Gd metal: $\gamma = 4.48 \pm 0.07 \text{ mJ}/(\text{g-at K}^2)$, $\delta = 1.37 \pm 0.06 \text{ mJ}/(\text{g-at K}^{5/2})$, and $\theta_D = 169 \pm 1$ K [32]. The Debye temperature is understandably higher in Gd_4ScGe_4 due to presence of covalentlike bonding between Ge atoms, while the electronic specific heat coefficient, considering the uncertainties, is comparable. The spin-wave or magnetic contributions appear to be higher in Gd_4ScGe_4 , which may explain a mild upturn in electrical resistivity below 3 K by the increased scattering of charge carriers on the magnetic moments – a similar yet weaker effect compared to the one observed above T_C , which is discussed next.

C. Electrical transport

The electrical resistivity of the Gd_4ScGe_4 crystal measured along the [100] direction is shown in Fig. 7. In addition to the zero-field electrical resistivity data shown in the Fig. 7(a),

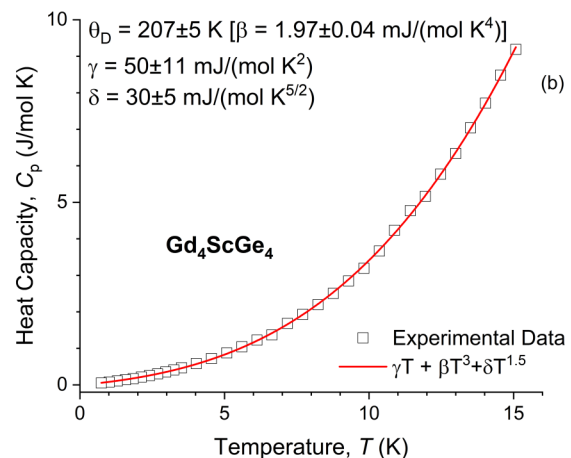


FIG. 6. Heat capacity of Gd_4ScGe_4 in zero applied magnetic field measured between 0.7 and 15 K: (a) C_p/T vs T^2 plot showing downward curvature at the lowest temperatures, the straight dashed line is a guide for the eye; (b) C_p vs T data fitted using the equation $C_p(T) = \gamma T + \beta T^3 + \delta T^{1.5}$.

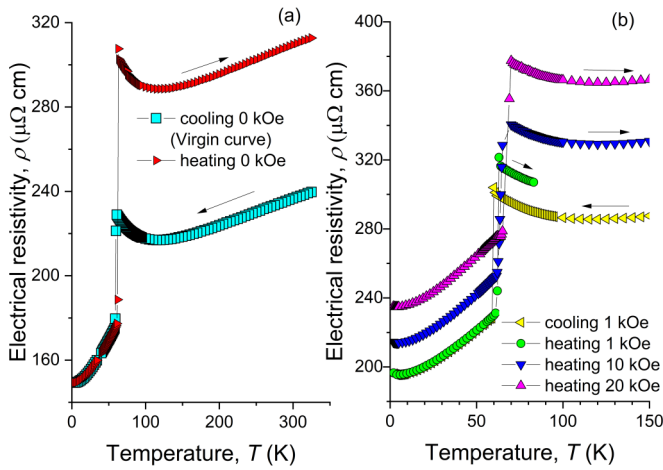


FIG. 7. Electrical resistivity of Gd_4ScGe in (a) zero magnetic field; (b) applied magnetic field of $H = 1, 10,$ and 20 kOe.

electronic transport measurements were also performed in applied magnetic fields up to 20 kOe [Fig. 7(b)]. One can see that the residual resistivity increases each time the sample crosses the first-order transition, which can be explained by the development of microcracks due to volume expansion/contraction associated with the transition (the largest discontinuous linear strain occurs along the a axis, and is exceeding $10\,000$ ppm) [21]. The repeated increase of residual resistivity due to cracking makes an accurate analysis of the temperature dependence of the electrical resistivity, $\rho(T)$, in the vicinity of the first-order transition difficult. Nevertheless, a number of interesting observations can be deduced.

First, the $\rho(T)$ dependence is for the most part metallic, in contrast with the $\rho(T)$ behavior of Gd_5Ge_4 reported by Levin *et al.* [13], and in agreement with our expectation of the more metallic behavior caused by the Sc substitutions. However, on approaching the transition (on cooling) the $\rho(T)$ reveals a gradual change from its conventional high-temperature metallic character towards anomalous behavior. As illustrated in the Fig. 8(b) the slope, $d\rho(T)/dT$, becomes

negative below 120 K. At T_C , resistivity drops abruptly reflecting the discontinuous nature of the phase transition, and the temperature dependence becomes metallic again except at the lowest temperatures, where a weak upturn in $\rho(T)$ is seen again below 3 K. The minor upturn can be also seen on the ^3He data collected from 0.7 to 10 K (not shown), although the data are somewhat noisy (the ^3He measurement was performed after the sample underwent multiple cycles, crossing T_C , at that point developing multiple stress-induced internal microcracks). Therefore, we could not analyze those low-temperature electrical resistivity data any further.

The application of magnetic field does not qualitatively change the electronic transport behavior of Gd_4ScGe . The continuing increase in the electrical resistivity values should be attributed to the gradually increasing residual resistivity due to cracking. In fact, when $\rho(T)$ data are normalized to their corresponding 150 K values [Fig. 8(a)], the $\rho(T)/\rho(150\text{ K})$ curves practically overlap above T_C (we note that the conventional approach of using resistivity at 2 K for normalizing data above T_C is less convenient here because the number of cracks increases when the transition is crossed). This is in contrast with the behavior observed in $\text{Gd}_5\text{Si}_{0.4}\text{Ge}_{3.6}$ [20], although in our study the number of cycles is smaller. The magnetic field, however, has a strong influence on T_C (defined as a maximum of $d\rho(T)/dT$, on heating), which increases from 62 K for 0 kOe to 69 K for the 20 kOe field. The transition temperature in a zero magnetic field is slightly lower in the electrical resistivity sample, which was cut from a different grain compared to the magnetic and heat capacity specimens, which indicates further enrichment in Gd compared to the nominal Gd_4Sc stoichiometry; the response to the magnetic field is, however, consistent with the $dT_C/dH = 0.35$ K/kOe observed in the magnetization measurements discussed above.

IV. DISCUSSION

According to Levin *et al.* [13], the negative $d\rho(T)/dT$ behavior above the antiferromagnetic ordering temperature,

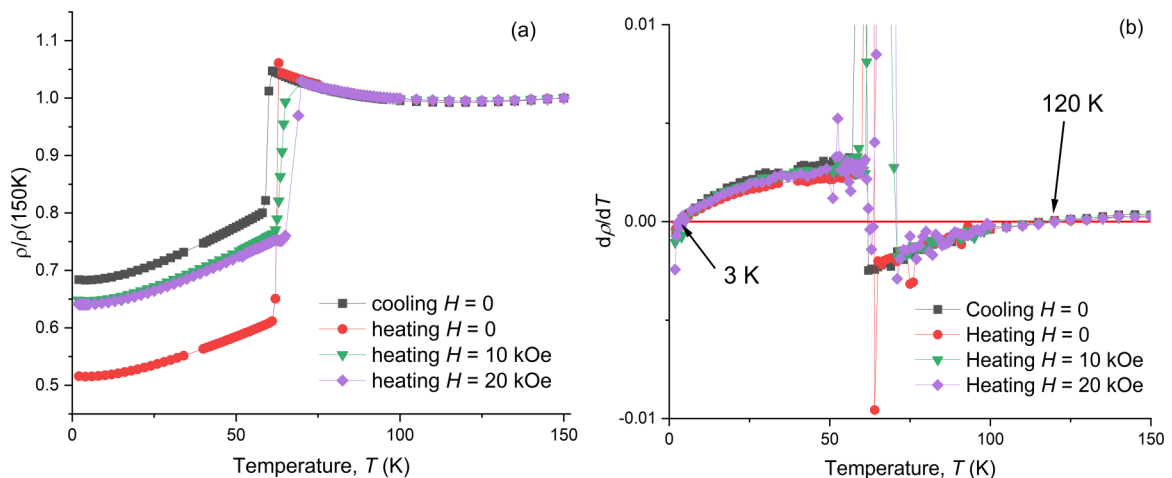


FIG. 8. (a) Temperature dependence of the $\rho(T)/\rho(150\text{ K})$ ratio in $0, 10,$ and 20 kOe applied magnetic fields; (b) $d\rho(T)/dT$ plots of the electrical resistivity data obtained in $0, 10,$ and 20 kOe applied magnetic fields shown to highlight the sign inversion at 3 and 120 K (large $d\rho(T)/dT$ values at the transition exceed the vertical scale of the plot).

$T_N = 130$ K, in Gd_5Ge_4 is best described in terms of hopping conductivity [$\rho \propto \exp(\frac{T_0}{T})^n$], with $n = 0.25$. Our initial hypothesis was that the electrical transport properties of the Sc-substituted Gd_5Ge_4 compounds would become more metallic compared to Gd_5Ge_4 , showing enhanced electric conductivity due to the presence of scandium's delocalized $3d$ electrons. This hypothesis is, indeed, validated by our experiments, which show that Gd_4ScGe_4 is, for the most part, conventionally metallic in the studied range of temperatures. At the same time, the presence of an extended region (between 63 and 120 K) where $d\rho(T)/dT < 0$ is certainly unusual and warrants a closer examination. This region (zero-field data) was analyzed using a number of different models earlier employed for Gd_5Ge_4 [13], including hopping conductivity ($\rho \propto \exp(T_0/T)^n$), Kondo scattering ($\rho \propto \ln T$), and thermally activated generation of charge carriers ($\ln \rho \propto 1/T$). None of the fits produces convincing results in the selected temperature range. In part, the failure to produce a successful fit may be attributed to the difficulty in the identification of the residual resistivity value for the high-temperature phase. However, we note that none of the listed models are best suited to describe the transport behavior of generally well-conducting intermetallics with a strong magnetic exchange and there is prevailing evidence that Gd_4ScGe_4 is a metal in both polymorphic modifications. Further, the O(I) state is clearly ferromagnetic and the Weiss temperature of the O(II) high-temperature phase is positive, $\theta_p = 33$ K, indicating that without structural transformation the O(II) phase would have, likely, ordered FM as well.

Qualitatively, the observed electrical resistivity behavior is similar to the one reported earlier for another rare-earth intermetallic with magnetostructural transformation, ErCo_2 [33], but the authors provided no explanation for the observed $d\rho/dT < 0$ above the T_C . A theoretical model developed by Fisher and Langer [34] postulates that short-range spin fluctuations near T_C should produce cusplike behavior in $\rho_{\text{mag}}(T)$. However, the Fisher-Langer theory predicts $d\rho/dT > 0$ for metallic compounds in the whole temperature interval [35]. The increase in the magnetic part of electrical resistivity on approaching T_C from the paramagnetic region is well documented in many rare-earth alloys [36]. In many cases, such increase is not sufficient to affect the sign of $d\rho/dT$, validating Fisher-Langer theory, but there is a number of notable exclusions, where sign reversal of $d\rho/dT$ has been observed; for example, in RCO_2 Laves phases, such as TmCo_2 [36] and aforementioned ErCo_2 [33]. The sign-reversal is consistent with the de Gennes-Friedel theory [37], which postulates that the peak in overall $\rho(T)$ at T_C , and not just in $\rho_{\text{mag}}(T)$, should exist at T_C in conventional ferromagnetic metals with large spin moments. For example, the electronic transport properties of the Gd metal, indeed, revealed sign reversal of $d\rho/dT$ and a peak in $\rho(T)$ above T_C in the temperature dependence of electrical resistivity measured along the c axis that was attributed to spin fluctuations above T_C ; a deviation from the Curie-Weiss behavior was noted as well [38]. The effect is, however, masked in a polycrystalline Gd [39].

The validity of the de Gennes-Friedel model [37] has been disputed in later studies [34,35] but for the lack of better alternative we label the observed $\rho(T)$ in Gd_4ScGe_4 above the T_C as a “de Gennes-Friedel-like behavior”, a definition borrowed from Alexander *et al.* [35]. We also note that the low-temperature shoulder of the peak in $\rho(T)$ cannot

be reliably observed in materials exhibiting magnetostructural transitions; furthermore, the mathematical approaches developed to analyze the critical phenomena are not applicable to the first-order transition. For example, in the case of de Gennes-Friedel behavior, electrical resistivity in the temperature region where $d\rho/dT < 0$ is expected to follow the $\rho \propto t \ln t$ relation [35], where $t = (T/T_C)^{-1}$, however, t cannot be accurately defined in first-order materials, since the “true” T_C of the high-temperature phase is generally not known. Thus, it appears that there is currently no theory to quantitatively explain the observed $\rho(T)$ in Gd_4ScGe_4 . However, we believe that the primary reason for the observed anomalous behavior is most likely related to the strong short-range spin interactions above T_C .

Considering the anomalous inverse magnetic susceptibility of Gd_4ScGe_4 above T_C [Fig. 4(b)] one can assume that the increased scattering of charge carriers (electrons) on either dynamic or static magnetic clusters is responsible for the $\rho(T)$ upturn. One may argue, however, that the application of magnetic field should, in principle, suppress the spin fluctuations [28–30]. Yet, our data measured in magnetic fields up to 20 kOe do not reveal any qualitative change in the $\rho(T)$ curvature above T_C compared to the zero-field data, the only change observed, in addition to the increase in residual resistivity, is the positive shift in T_C [Fig. 8(a)], in agreement with the magnetic data. Short-range clusters, therefore, persist in higher magnetic fields as well but their presence is masked by the increased paramagnetic response of the matrix.

While the rise in electron-paramagnon scattering can be invoked to explain the increase in $\rho(T)$ with decreasing temperature, because the transition at T_C is magnetostructural, we should also consider the effect of the increased electron-phonon scattering near the T_C . By plotting the temperature dependence of the interslab $d(\text{Ge3-Ge3})$ atomic distance of Gd_4ScGe_4 using the data from Ref. [21], anomalous behavior of $d(\text{Ge3-Ge3})$ is clearly evident above T_C . Namely, this (critical) interslab distance increases right before (on cooling) and after (on heating) the structural transformation occurs (see Fig. 9), matching the behavior of the $\rho(T)$ curve. A similar “spike” was observed in $\text{Gd}_5\text{Si}_{0.5}\text{Ge}_{3.5}$ [23], and the presence of intermediate structural states in related Er_5Si_4 has been postulated based on the detailed temperature-dependent crystallographic study of the Er_5Si_4 single crystal [40]. Thus, the “softening” of the lattice in the vicinity of the transition and the presence of intermediate states must contribute to the increased carrier scattering (lower mean path) and lower electrical conductivity of the material, in addition to the electron-paramagnon scattering.

The increase in electrical resistivity at low temperatures is reminiscent of the upturn that occurs above T_C . While the material is fully FM ordered below 3 K, we note that the fitting of the heat capacity data indicates the presence of magnetic contribution in addition to the lattice and electronic terms. This contribution is likely associated with magnons or spin waves. We also note that the anomalous nature of $\rho(T)$ behavior at $T < 3$ K does not seem to be qualitatively affected by cycling. Thus, we suggest that the electron-magnon scattering, similarly to the electron-paramagnon scattering above T_C , becomes notable in the $\rho(T)$ behavior, once the electrical resistivity stops decreasing due to FM ordering.

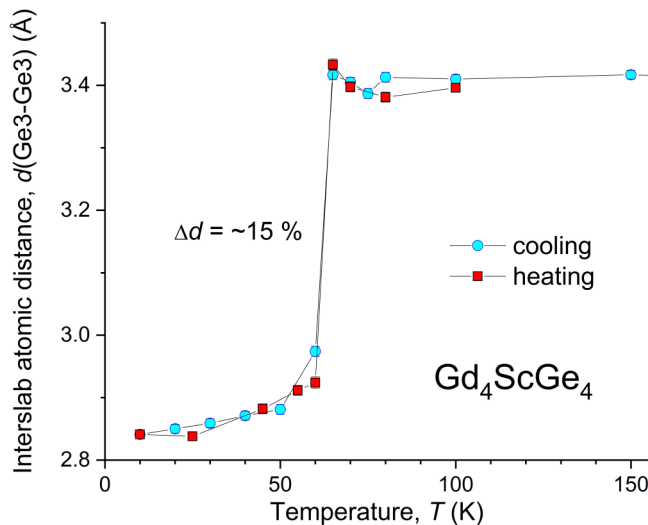


FIG. 9. Temperature dependence of the interslab interatomic distance Ge3-Ge3 [$d(T-T)$ in Fig. 1] plotted using the Rietveld-refined data from Ref. [21].

V. CONCLUSIONS

Physical property measurements of the Gd_4ScGe_4 single-crystal indicate a strong influence of spin interactions on the magnetic and electrical transport properties above the magnetostructural transition temperature, T_C . The hopping

conductivity phenomenon, previously reported for Gd_5Ge_4 , is not observed in Gd_4ScGe_4 and the $\rho(T)$ dependence is mostly metallic, with the exception of the regions between $T_C = 63$ and 120 K, as well as below 3 K, where the electrical resistivity, ρ , increases with the decreasing temperature. We suggest that both electron-paramagnon and electron-phonon scattering enhancement causes the observed anomalous $\rho(T)$ behavior above T_C . Heat capacity confirms strong spin-wave contributions at low temperatures, suggesting that the upturn in $\rho(T)$ below 3 K is related to the electron-magnon scattering. The experimental data also confirm a strong discontinuous first-order nature of the magnetostructural transition at $T_C = 63$ K in Gd_4ScGe_4 . Minor magnetocrystalline anisotropy is detected, with the b axis as the easy magnetization direction. There is a minor additional contribution to the total magnetization, which is dominated by the Gd $4f$ local moments, from the nominally nonmagnetic Sc due to spin polarization of conduction electrons.

ACKNOWLEDGMENTS

This work performed at Ames Laboratory was supported by the Division of Materials Science and Engineering of the Office of Basic Energy Sciences of the U.S. Department of Energy (DOE). Ames Laboratory is operated for the U.S. DOE by Iowa State University under Contract No. DE-AC02-07CH11358.

- [1] R. Kainuma, Y. Imano, W. Ito, Y. Sutou, H. Morito, S. Okamoto, O. Kitakami, K. Oikawa, A. Fujita, T. Kanomata, and K. Ishida, Magnetic-field-induced shape recovery by reverse phase transformation, *Nature (London)* **439**, 957 (2006).
- [2] J. Liu, T. Gottschall, K. P. Skokov, J. D. Moore, and O. Gutfleisch, Giant magnetocaloric effect driven by structural transitions, *Nature Mater.* **11**, 620 (2012).
- [3] B. Raveau, A. Maignan, C. Martin, and M. Hervieu, Colossal magnetoresistance manganite perovskites: Relations between crystal chemistry and properties, *Chem. Mater.* **10**, 2641 (1998).
- [4] V. K. Pecharsky and K. A. Gschneidner, Jr., $\text{Gd}_5(\text{Si}_x\text{Ge}_{1-x})_4$: An extremum material, *Adv. Mater.* **13**, 683 (2001).
- [5] V. K. Pecharsky, A. P. Holm, K. A. Gschneidner, Jr., and R. Rink, Massive Magnetic-Field-Induced Structural Transformation in Gd_5Ge_4 and the Nature of the Giant Magnetocaloric Effect, *Phys. Rev. Lett.* **91**, 197204 (2003).
- [6] V. K. Pecharsky and K. A. Gschneidner, Jr., Giant Magnetocaloric Effect in $\text{Gd}_5(\text{Si}_2\text{Ge}_2)$, *Phys. Rev. Lett.* **78**, 4494 (1997).
- [7] L. Morellon, P. A. Algarabel, M. R. Ibarra, J. Blasco, B. García-Landa, Z. Arnold, and F. Albertini, Magnetic-field-induced structural phase transition in $\text{Gd}_5(\text{Si}_{1.8}\text{Ge}_{2.2})$, *Phys. Rev. B* **58**, R14721 (1998).
- [8] Y. Mudryk, V. K. Pecharsky, and K. A. Gschneidner, Jr., Extraordinary responsive intermetallic compounds: The R_5T_4 family ($R = \text{rare earth}$, $T = \text{group 13-15 element}$), *Z. Anorg. Allg. Chem.* **637**, 1948 (2011).
- [9] Ya. Mudryk, Y. Lee, T. Vogt, K. A. Gschneidner, Jr., and V. K. Pecharsky, Polymorphism of $\text{Gd}_5\text{Si}_2\text{Ge}$: The equivalence of temperature, magnetic field, and chemical and hydrostatic pressures, *Phys. Rev. B* **71**, 174104 (2005).
- [10] Ya. Mudryk, A. P. Holm, K. A. Gschneidner, Jr., and V. K. Pecharsky, Crystal structure-magnetic property relationships of Gd_5Ge_4 examined by *in situ* x-ray powder diffraction, *Phys. Rev. B* **72**, 064442 (2005).
- [11] S. B. Roy, M. K. Chattopadhyay, P. Chaddah, J. D. Moore, G. K. Perkins, L. F. Cohen, K. A. Gschneidner, Jr., and V. K. Pecharsky, Evidence of a magnetic glass state in the magnetocaloric material Gd_5Ge_4 , *Phys. Rev. B* **74**, 012403 (2006).
- [12] S. Velez, J. M. Hernandez, A. Fernandez, F. Macia, C. Magen, P. A. Algarabel, J. Tejada, and E. M. Chudnovsky, Magnetic deflagration in Gd_5Ge_4 , *Phys. Rev. B* **81**, 064437 (2010).
- [13] E. M. Levin, V. K. Pecharsky, K. A. Gschneidner, Jr., and G. J. Miller, Electrical resistivity, electronic heat capacity, and electronic structure of Gd_5Ge_4 , *Phys. Rev. B* **64**, 235103 (2001).
- [14] C. Magen, L. Morellon, P. A. Algarabel, C. Marquina, and M. R. Ibarra, Magnetoelastic behavior of Gd_5Ge_4 , *J. Phys.: Condens. Matter* **15**, 2389 (2003).
- [15] Y. Mudryk, V. K. Pecharsky, and K. A. Gschneidner, Jr., R_5T_4 compounds. An extraordinary versatile model system for the solid state science, in *Handbook on the Physics and Chemistry of Rare Earths*, edited by J.-C. Bunzli, and V. K. Pecharsky (Elsevier, Amsterdam, 2014), Vol. 44, pp. 283–449.

- [16] J. Szade and G. Skorek, Electronic structure and magnetism of $Gd_5(Si, Ge)_4$ compounds, *J. Magn. Magn. Mater.* **196–197**, 699 (1999).
- [17] Y. Xue, Z. Chen, X. Zhang, Y. Su, S. Cao, and J. Zhang, Dependence of magnetization on temperature, magnetoresistance effect and magnetic phase diagram for the layered Gd_5Ge_4 compound, *J. Supercond. Nov. Magn.* **22**, 637 (2009).
- [18] G. Skorek, J. Deniszczuk, and J. Szade, Electronic structure of $Gd_5(Si, Ge)_4$, *J. Phys.: Condens. Matter.* **14**, 7273 (2002).
- [19] L. Morellon, J. Blasco, P. A. Algarabel, and M. R. Ibarra, Nature of the first-order antiferromagnetic-ferromagnetic transition in the Ge-rich magnetocaloric compounds $Gd_5(Si_xGe_{1-x})_4$, *Phys. Rev. B* **62**, 1022 (2000).
- [20] J. B. Sousa, M. E. Braga, F. C. Correia, F. Carpintero, L. Morellon, P. A. Algarabel, and M. R. Ibarra, Anomalous behavior of the electrical resistivity in the giant magnetocaloric compound $Gd_5(Si_{0.1}Ge_{0.9})_4$, *Phys. Rev. B* **67**, 134416 (2003).
- [21] Y. Mudryk, D. Paudyal, J. Liu, and V. K. Pecharsky, Enhancing magnetic functionality with scandium: Breaking stereotypes in the design of rare earth materials, *Chem. Mater.* **29**, 3962 (2017).
- [22] J. Liu, Y. Mudryk, V. Smetana, A.-V. Mudring, and V. K. Pecharsky, Anomalous effects of Sc substitution and processing on magnetism and structure of $(Gd_{1-x}Sc_x)_5Ge_4$, *J. Magn. Magn. Mater.* **474**, 482 (2019).
- [23] Ya. Mudryk, D. Paudyal, V. K. Pecharsky, and K. A. Gschneidner, Jr., Magnetostructural transition in $Gd_5Si_{0.5}Ge_{3.5}$: Magnetic and x-ray powder diffraction measurements, and theoretical calculations, *Phys. Rev. B* **77**, 024408 (2008).
- [24] J. Rodriguez-Carvajal, Recent advances in magnetic structure determination by neutron powder diffraction, *Physica B* **192**, 55 (1993).
- [25] D.-X. Chen, E. Pardo, and A. Sanchez, Demagnetizing factors for rectangular prisms, *IEEE Trans. Magn.* **41**, 2077 (2005).
- [26] Z. W. Ouyang, V. K. Pecharsky, K. A. Gschneidner, Jr., D. L. Schlagel, and T. A. Lograsso, Magnetic anisotropy and magnetic phase diagram of Gd_5Ge_4 , *Phys. Rev. B* **74**, 024401 (2006).
- [27] L. Tan, A. Kreyssig, J. W. Kim, A. I. Goldman, R. J. McQueeney, D. Wermeille, B. Sieve, T. A. Lograsso, D. L. Schlagel, S. L. Budko, V. K. Pecharsky, and K. A. Gschneidner, Jr., Magnetic structure of Gd_5Ge_4 , *Phys. Rev. B* **71**, 214408 (2005).
- [28] Z. W. Ouyang, V. K. Pecharsky, K. A. Gschneidner, Jr., D. L. Schlagel, and T. A. Lograsso, Short-range anisotropic ferromagnetic correlations in the paramagnetic and antiferromagnetic phases of Gd_5Ge_4 , *Phys. Rev. B* **74**, 094404 (2006).
- [29] C. Magen, P. A. Algarabel, L. Morellon, J. P. Araujo, C. Ritter, M. R. Ibarra, A. M. Pereira, and J. B. Sousa, Observation of a Griffiths-like Phase in the Magnetocaloric Compound Tb_5Si_2Ge , *Phys. Rev. Lett.* **96**, 167201 (2006).
- [30] A. M. Pereira, L. Morellon, C. Magen, J. Ventura, P. A. Algarabel, M. R. Ibarra, J. B. Sousa, and J. P. Araujo, Griffiths-like phase of magnetocaloric $R_5(Si_xGe_{1-x})_4$ ($R = Gd, Tb, Dy, \text{ and Ho}$), *Phys. Rev. B* **82**, 172406 (2010).
- [31] P. Wells, P. C. Lanchester, D. W. Jones, and R. G. Jordan, The specific heat of high purity gadolinium between 1.5 and 14 K, *J. Phys. F* **4**, 1729 (1974).
- [32] R. W. Hill, S. J. Collocott, K. A. Gschneidner, Jr., and F. A. Schmidt, The heat capacity of high-purity gadolinium from 0.5 to 4 K and the effects of interstitial impurities, *J. Phys. F: Metal Phys.* **17**, 1867 (1987).
- [33] M. Misek, J. Prokleska, V. Sechovsky, D. Turcinkova, J. Prchal, A. F. Kusmartseva, K. V. Kamenev, and J. Kamarad, Effect of high pressure on the magnetism of $ErCo_2$, *J. Appl. Phys.* **111**, 07E132 (2012).
- [34] M. E. Fisher and J. S. Langer, Resistive Anomalies at Magnetic Critical Points, *Phys. Rev. Lett.* **20**, 665 (1968).
- [35] S. Alexander, J. S. Helman, and I. Balberg, Critical behavior of the electrical resistivity in magnetic systems, *Phys. Rev. B* **13**, 304 (1976).
- [36] E. Gratz, R. Resel, A. T. Burkov, E. Bauer, A. S. Markosyan, and A. Galatanu, The transport properties of RCO_2 compounds, *J. Phys.: Condens. Matter* **7**, 6687 (1995).
- [37] P. G. de Gennes and J. Friedel, Anomalies de resistivite dans certains metaux magnetiques (in French), *J. Phys. Chem. Solids* **4**, 71 (1958).
- [38] H. E. Nigh, S. Legvold, and F. H. Spedding, Magnetization and electrical resistivity of gadolinium single crystals, *Phys. Rev.* **132**, 1092 (1963).
- [39] R. V. Colvin, S. Legvold, and F. H. Spedding, Electrical resistivity of heavy rare earth metals, *Phys. Rev.* **120**, 741 (1960).
- [40] Y. Mozharivskiy, A. O. Pecharsky, V. K. Pecharsky, G. J. Miller, and K. A. Gschneidner, Jr., Tracking and understanding the first-order structural transition in Er_5Si_4 , *Phys. Rev. B* **69**, 144102 (2004).